Landsat-based greening trends in alpine ecosystems are inflated by multidecadal increases in summer observations

Arthur Bayle, Simon Gascoin, Logan T Berner, Philippe Choler

ECOGRAPHY

Research article

Landsat-based greening trends in alpine ecosystems are inflated by multidecadal increases in summer observations

Arthur Bayle[1], **Simon Gascoin**[2], **Logan T. Berner**[3] and **Philippe Choler**[1]

[1]Univ. Grenoble Alpes, Univ. Savoie Mont Blanc, CNRS, LECA, Grenoble, France
[2]Univ. Toulouse, CESBIO, CNES CNRS IRD INRAE UT3 Paul Sabatier, Toulouse, France
[3]School of Informatics, Computing and Cyber Systems, Northern Arizona University, Flagstaff, AZ, USA

Correspondence: Arthur Bayle (arthur.bayle.env@gmail.com)

Ecography
2024: e07394
doi: 10.1111/ecog.07394
Subject Editor: Jian Zhang
Editor-in-Chief: Miguel Araújo
Accepted 22 July 2024

Remote sensing is an invaluable tool for tracking decadal-scale changes in vegetation greenness in response to climate and land use changes. While the Landsat archive has been widely used to explore these trends and their spatial and temporal complexity, its inconsistent sampling frequency over time and space raises concerns about its ability to provide reliable estimates of annual vegetation indices such as the annual maximum normalised difference vegetation index (NDVI), commonly used as a proxy of plant productivity. Here we demonstrate for seasonally snow-covered ecosystems, that greening trends derived from annual maximum NDVI can be significantly overestimated because the number of available Landsat observations increases over time, and mostly that the magnitude of the overestimation varies along environmental gradients. Typically, areas with a short growing season and few available observations experience the largest bias in greening trend estimation. We show these conditions are met in late snowmelting habitats in the European Alps, which are known to be particularly sensitive to temperature increases and present conservation challenges. In this critical context, almost 50% of the magnitude of estimated greening can be explained by this bias. Our study calls for greater caution when comparing greening trends magnitudes between habitats with different snow conditions and observations. At a minimum we recommend reporting information on the temporal sampling of the observations, including the number of observations per year, when long-term studies with Landsat observations are undertaken.

Keywords: alpine, bias, greening, Landsat, observations, tundra

Introduction

Satellite remote sensing (SRS) has become an indispensable tool for deriving biophysical parameters of terrestrial and oceanic ecosystems at spatial scales unattainable through other observation methods (Randin et al. 2020, Loveland et al. 2022, Wulder et al. 2022). The emergence of open and up-to-date data has made it possible to address

NORDIC SOCIETY OIKOS
www.ecography.org

environmental changes at the core of the 21st century climate and biodiversity crises by monitoring key biophysical parameters across Earth's surface (Wulder et al. 2022). Vegetation greening, defined as a 'positive trend in vegetation greenness', stands as one the most striking example of human-induced change that is historically intertwined with advances in satellite remote sensing (Tucker and Sellers 1986, Piao et al. 2019, Shukla et al. 2019). Research from the 1970s revealed close connections between the remotely sensed normalised difference vegetation index (NDVI) and plant photosynthetic activity (Rouse et al. 1974, Tucker 1979), an insight that allowed scientists to monitor changes in vegetation greenness at global scales and in areas often challenging to access. In a seminal study, Myneni et al. (1997) reported increases in vegetation greenness in the Northern Hemisphere using coarse resolution satellite observations. Subsequently studies revealed with unequivocal result: the land surface has been greening over the last four decades at regional and continental scales (Goetz et al. 2005, Krishnaswamy et al. 2014, Zhu, X. et al. 2016, Zhu, Z. et al. 2016, Anderson et al. 2020, Myers-Smith et al. 2020, Choler et al. 2021). Recent research has used higher-resolution satellite observations due to growing evidence that vegetation responses are scale-dependent, the necessity to better link fine-scale ecological processes to remotely sensed patterns and trends, and increased computation power (Assmann et al. 2020, Berner et al. 2020, Myers-Smith et al. 2020).

The Landsat satellites are invaluable for tracking variability in fine-scale biophysical parameters at climate and ecologically relevant timescales, thanks to their high spatial resolution and extensive historical archive (Wulder et al. 2019). This holds particularly true in topographically heterogeneous landscapes such as mountains, as complex topography compresses life zones, thus juxtaposing diverse biological communities in close proximity (Choler 2018). The Landsat archive provides well-calibrated (Markham and Helder 2012) and precisely geolocated measurements (Lee et al. 2004, Masek et al. 2020); however, observation availability is highly irregular over space and time (Zhang et al. 2022), which complicates efforts to monitor biophysical parameters across Earth's surface (Berner et al. 2020). Over the past four decades, the quantity of usable observations collected by the optical sensors onboard Landsat satellites has drastically varied (Arvidson et al. 2006, Goward et al. 2006, Ju and Roy 2008, Kovalskyy and Roy 2013, Wulder et al. 2016, Zhang et al. 2022). For instance, Landsat 5, launched in 1984, faced communication issues due to equipment failures in 1988 and 1992, limiting acquisitions to times when the satellite was in direct view of an international ground station. With the 1999 launch of Landsat 7 two satellites operated simultaneously, allowing for eight-day coverage, though this was hampered by scan line corrector (SLC) failure in 2003, causing data gaps amounting to approximately 22% of the scene area. Additionally, Landsat 7 adopted a long-term acquisition plan resulting in the collection of at least one clear scene for each season globally every year (Arvidson et al. 2006). In 2013, with the decommissioning of Landsat 5 and the launch of Landsat 8, two satellites again collected imagery, both under efficient acquisitions plans. Observations are expected to increase even more with Landsat 9 as it is the first time in the Landsat era when two satellites are concomitantly operating without technical failures. Overall, the frequency of usable Landsat observations has varied, with fewer observations in the 1980s than in recent decades, and strong spatial variations due to cloudiness or snow (Zhang et al. 2022). Figure 1 illustrates spatial and temporal variability in available clear-sky and snow-free Landsat observations data from 1984 to 2021 in Landsat Collection 2 for summer months (June, July and August, referred to as the growing season) over the European Alps.

Due to their inherent seasonal variability, the characterization of biophysical parameters is affected by the sampling frequency of observations. The shorter the duration of the phenomena (i.e. seasonality), the greater the need for frequent sampling to obtain relevant measurements (Mallat and Hwang 1992). This is particularly true in seasonally snow-covered Arctic and alpine ecosystems, where the occurrence of peak standing biomass represents a brief period during the growing season, making the probability of capturing its full extent dependent on observation frequency. Vegetation greenness trends are typically estimated using single-rule maximum compositing algorithms applied annually throughout the time series (Holben 1986, Qiu et al. 2023). However, with the Landsat time series showing increased sampling frequency over time, recent years are more likely to capture the peak of greenness (Berner et al. 2020). The widespread availability of Landsat data on cloud-computing platforms like Google Earth Engine has exposed a broad user base to this issue, underscoring the need for better understanding of its mechanisms and potential consequences on environmental studies. Although the concept of this maximum NDVI sampling bias is acknowledged and methods for its correction have been proposed (Karlsen et al. 2018, Berner et al. 2020, 2023, Wang et al. 2022), demonstrations to date have focused only on the relationship between the estimated maximum NDVI and the number of observations (Berner et al. 2020, 2023). Nevertheless, no studies have thoroughly evaluated or quantified how the maximum NDVI sampling bias impacts the magnitude of greening trends, the factors influencing its magnitude, and the potential consequences on our understanding of plant dynamics. This raises three key questions: how does maximum NDVI sampling bias affect Landsat-based greening trend estimates? Also, what parameters influence the magnitude of this bias and to what extent? Which plant communities are most affected and to what extent may this lead to misleading interpretation when comparing changes in plant communities? This paper addresses these questions in the case of the European Alps.

Data, methods and analysis

Our analysis is structured in three parts, each corresponding to a research question, with the complete procedure described in the Supporting information.

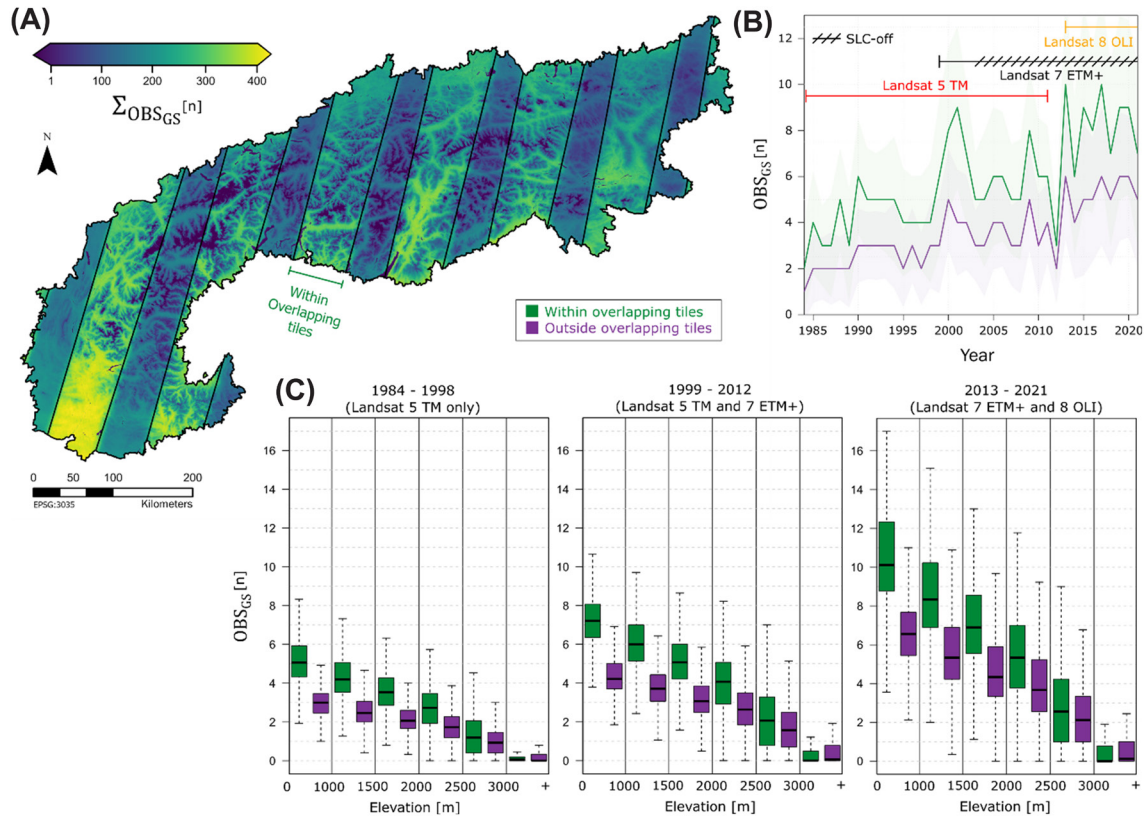

Figure 1. Spatio-temporal distribution of clear-sky and snow-free Landsat observations during the growing season in the European Alps. (A) Sum of observations from 1984 to 2021 for the entire European Alps as defined by the Alpine Convention (www.alpconv.org). Landsat paths are shown in black stripes. (B) Mean number and standard deviation of clear-sky and snow-free Landsat observations during the growing season from 1984 to 2021 within and outside overlapping tiles. (C) Distribution of clear-sky and snow-free Landsat observations during the growing season along an elevation gradient for the three Landsat periods (Landsat 5 TM only, Landsat 5 TM and 7 ETM+ combined, and Landsat 7 ETM+ and 8 OLI combined) differentiating between zones within and outside overlapping tiles. The C Version of Function of Mask (CFmask) was applied to define the attributes of the pixel qualities, which identified each pixel as clear (land/water), snow, cloud, adjacent to cloud, or cloud shadow (Zhu and Woodcock 2012). Elevation was obtained using the 25 × 25 m resolution EU-DEM resampled to the Landsat grid of 30 × 30 m resolution using bilinear interpolation. See the Supporting information for similar analysis in the Arctic tundra and Asian mountain ranges.

Quantification of false greening trends over the European Alps using Landsat

Answering question 1 (in what ways and to what extent does NDVImax sampling bias impact the estimates of Landsat-based greening trends?) requires characterizing the 1) underlying vegetation phenological curves and 2) scenarios of Landsat usable observations over the European Alps, for which we used MODIS and Landsat datasets, respectively. To summarize the procedure described in this section: 1) the daily NDVI time series from MODIS allows us to obtain a precise phenology; 2) we then use this phenology to sample NDVI values from the Landsat time series observation density; 3) from these NDVI values, we derive the maximum NDVI for each year; and 4) we calculate the 38-year trend in these NDVImax values. Assuming that Landsat provides one observation per day, we would consistently capture the same NDVImax from year to year, resulting in no detected trend. Therefore, obtaining an NDVImax slope in this case amounts to measuring the effect of sampling density alone on the NDVImax trend. This entire procedure is repeated for each of the three vegetation clusters.

To characterize vegetation phenology, we used the 250-m resolution eight-day composite of MODIS MOD09QA/Terra collection six products over the entire European Alps (n = 1 076 872 pixels). MODIS has daily acquisition which enables a more in-depth characterisation of land surface phenology in comparison to Landsat with its coarser temporal resolution. Acquired dates spanned from 18 February 2000 to 27 December 2021. We assembled tiles h18v4 and h19v04 to cover the entire mountain range and reprojected red (RED) and near-infrared (NIR) surface reflectance values for high quality pixels (according to the MOD09QA quality control flag) and calculated NDVI according to (NIR-RED)/(NIR+RED). We limited the analysis to pixels with non-forested land cover classes, tree cover density below 5%, elevation above 1500 m, and an NDVImax above 0.1 (Fig. 2A). To do so, we employed the 25-m resolution digital elevation model and the 100-m resolution tree cover density of year 2018

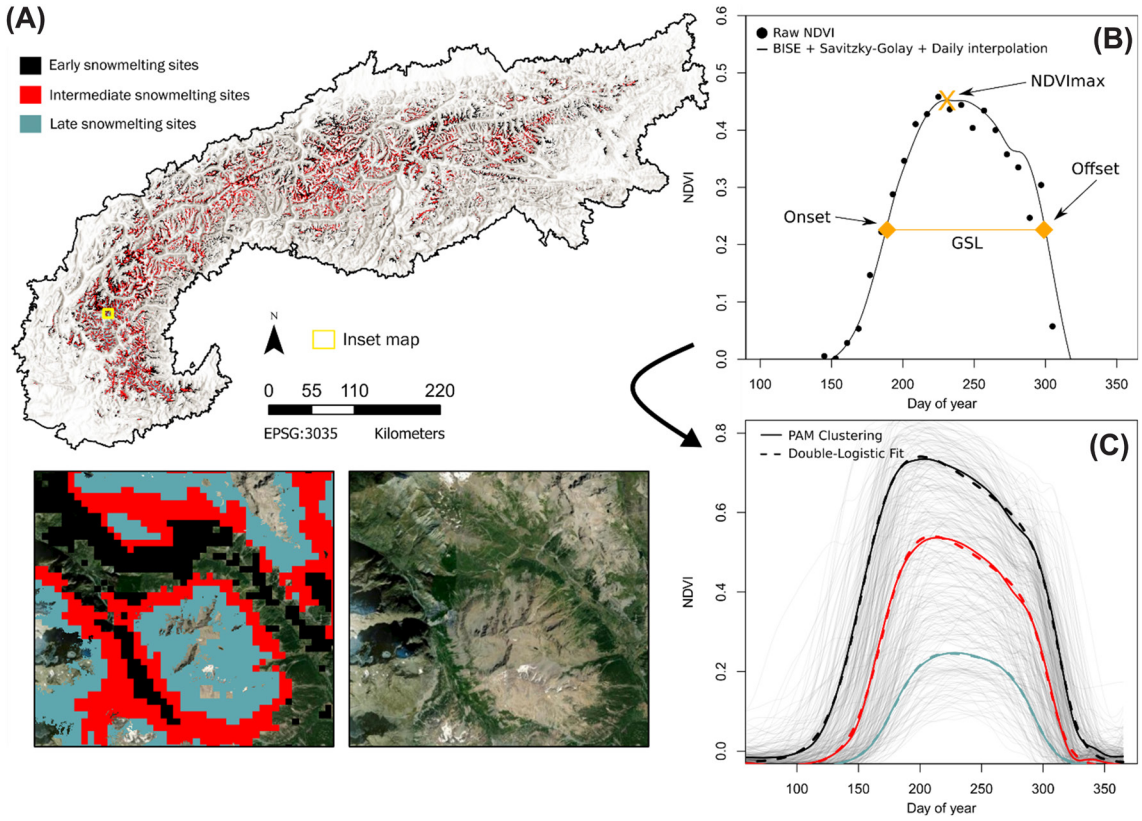

Figure 2. (A) Spatial distribution of phenological clusters in the European Alps with inset maps over the Lautaret Pass, France. Non-coloured areas represent areas that did not match criteria for inclusion. (B) Raw, and interpolated MODIS-derived NDVI time series for a random point in the European Alps with indication of phenological metrics extracted for the analysis. (C) Full lines represent daily interpolated MODIS-derived NDVI time series for early (black), intermediate (red), and late (blue) snowmelting sites obtained from PAM clustering. Dashed lines represent the corresponding seven-parameters double logistic fits. Shaded curves represent pixel curves.

(https://land.copernicus.eu/pan-european/high-resolution-layers/forests/tree-cover-density). For each remaining pixel (n = 546 273), we merged all years into one annual time series to obtain a median representation of vegetation phenology. We then processed the raw NDVI time series in two steps. First, we used the best index slope extraction (BISE) algorithm to reduce the noise of the NDVI time series (Viovy et al. 1992) applied a low-pass filter using the Savitzky–Golay algorithm (Savitzky and Golay 1964). We then interpolated daily NDVI using the spline method. For representation purposes only, we implemented a partitioning around medoids (PAM) model for n = 30 000 NDVI time series using a number of K = 4 clusters (Fig. 2). Cluster 1 was discarded because it exhibited high NDVI values during the winter season, likely due to the presence of forest or tall shrub patches. Increasing the number of prescribed clusters led to intermediate phenologies and did not significantly enhance the clarity of results displayed. The model was then used to calculate the distances between medoids, and the entire dataset and each pixel of the European Alps was assigned to the closest medoid. We interpreted the three vegetation clusters as early, intermediate, and late snowmelt sites based on their elevation distribution and growing season length and used these terminologies hereafter (Fig. 2C).

For each cluster, we fitted a seven-parameter double logistic (DL) function (Supporting information). We employed DL models instead of MODIS-NDVI time series to mathematically characterize these phenologies, thereby increasing the reproducibility of our analysis based on a widely used phenological model. The R package 'Cluster' was used to assign pixels to clusters (Maechler et al. 2022). The fitting was performed using the GENOUD (GENetic optimization using derivatives) algorithm implemented in the 'rgenoud' package (Mebane and Sekhon 2011).

To quantify the actual availability of Landsat observations over time, we extracted annual time series of the number of clear-sky and snow-free Landsat observations during the growing season (OBS_{GS}) from GEE by applying the CFmask to remove snow, clouds, and cloud shadows from Landsat 5 TM, 7 ETM+ and 8 OLI images (Collection 2) between day of year (DOY) 152–243 (Zhu and Woodcock 2012) over the European Alps. Annual time series of OBS_{GS} were applied to a simulated Landsat acquisition sequence with an acquisition every eight days over a year to obtain annual time series of NDVImax. For instance, if a pixel had three observations available during a given year, then we randomly drew three daily MODIS NDVI values from the acquisition dates between DOY 152 and 243 and computed the maximum

NDVI values. Because the phenological data were distributed on a 250-m resolution grid while Landsat observations were distributed on a 30-m resolution grid, we systematically used the Landsat pixel landing on the centroid of the MODIS pixel to associate both datasets without resampling.

To confirm the asymptotic relationship between OBS_{GS} and NDVImax initially observed by Berner et al. (2020), we randomly sampled a gradually increasing number of observations (from 1 to 8) during the growing season (DOY 152–243) and estimated the NDVImax for each scenario. This allowed us to compute the discrepancy between the estimated NDVImax and the 'true' NDVImax obtained from the DL model fit to the daily MODIS NDVI timeseries. This procedure was repeated for the three phenological clusters to test the impact of phenological variation on NDVImax sampling. We evaluated the impact of changing the starting date (resulting in seven possible chronosequences with the first day being day 1, 2, 3, … 7) and the revisit time before sampling (4, 8 or 16 days) on the generated Landsat observation time series and found no impact on the results (Supporting information). We also performed the analysis using quantile metrics (median, q75, q80 and q90) instead of maximum to derive annual vegetation greenness in order to test for similarity in the sampling bias behaviour. Specifically, we tested the nine methods to compute quantiles as listed in Hyndman and Fan (1996). Finally, we tested for the effect of randomizing observation dates compared to using the actual DOY for every observation. More details on these analyses are available in the Supporting information.

To address our first question, we generated annual NDVImax time series by creating a 38-year stable (i.e. no trend) NDVI time series for each of the three vegetation clusters (absence of NDVImax trends by sampling true NDVImax). The 38-year stable NDVI time series was obtained by simply repeating the same annual NDVI phenology curve 38 times. Then, we subsampled each NDVI time series using the annual time series of OBS_{GS}, and then calculated temporal trends in NDVImax based on subsampled time series. Trends in NDVImax, hereafter referred to as absolute 'false trends' ($a\beta_F$), were estimated using the Theil–Sen parameter. We relied on a simple Theil–Sen slope estimator to determine the magnitude of temporal trends because those methods are robust against outliers and widely used by the community despite acknowledgements that there is issue of temporal autocorrelation (Ives et al. 2021). In addition, as we are focusing solely on slope estimation and not p-values, temporal autocorrelation is not expected to be an issue in our analysis. Because there was no trend in the true NDVImax time series, we know that $a\beta_F$ estimates are solely the result of variation in OBS_{GS} and phenology. In addition, we computed the relative ($r\beta_F$) as a measure of importance of $a\beta_F$, using the following formula:

$$r\beta_F = \left(\left(\frac{a\beta_F}{NDVImax}\right)\times 100\right)\times n$$

with n as the number of years in the time series (n = 38) and NDVImax depending on the true NDVImax.

Phenological and observational drivers of spatial variability in the magnitude of false trends

To answer question 2 (which parameters are driving the magnitude of false trends, and to what extent?), we extracted 100 time series of NDVI and 100 000 time series of OBS_{GS} from datasets described in section 'Quantification of false greening trends over the European Alps using Landsat' and computed $a\beta_F$ for each combination (n = 10 000 000 estimates of $a\beta_F$). Time series of NDVI (phenological curves) were obtained by clustering n = 30 000 NDVI times series into K = 100 clusters as described in section 'Quantification of false greening trends over the European Alps using Landsat'. We used 100 clusters instead of four in order to increase the gradient of phenological curves on which to compute our model. We used this approach instead of directly using random time series of NDVI to reduce noise and obtain a larger number of representative phenologies for mountain vegetation growing season length in the European Alps. We extracted the onset and offset (defined as the first and last date of the year when the NDVI amounts 50% of the NDVImax) which was used to obtain the growing season length (GSL) (Fig. 2B). We summarized time series of annual OBS_{GS} by its sum ($\Sigma_{OBS_{GS}}$, as presented in Fig. 1). As a result, we obtained a list of $a\beta_F$ as a function of the following predictive variables: GSL and $\Sigma_{OBS_{GS}}$, which we used to build a random forest regression model, with R^2 as a measure of performance (Breiman 2001). We measured the relative variable importance using the percentage of increase in accuracy through out-of-bag approach. Then, we used partial dependence plot to show the marginal effect the two variables have on $a\beta_F$.

False trends and its relative importance along environmental and floristic gradients

To answer question 3 (how false trends are distributed along elevation and floristic gradients?), we extracted the GSL and $\Sigma_{OBS_{GS}}$ for every pixel and used the random forest regression model described in section 'Phenological and observational drivers of spatial variability in the magnitude of false trends' to obtain $a\beta_F$ at the scale of the European Alps and investigate its spatial distribution. We derived $r\beta_F$ from $a\beta_F$ as described in section 'Quantification of false greening trends over the European Alps using Landsat'. We computed the actual Landsat-based greening trends from 1984 to 2021 to quantify the relative importance of false trends compared to observed trends. To do that, we aligned reflectance measurements from Landsat 8 OLI to Landsat 7 ETM+ using the correction method described by Roy et al. (2016a). Also, we applied the c-factor approach to correct for bidirectional reflectance distribution function (BRDF) effects (Roy et al. 2016b). We estimated the yearly NDVImax and computed vegetation greenness trends ($\beta_{NDVImax}$) as described in section 'Quantification of false greening trends over the European Alps using Landsat'. Finally, we computed the relative importance of false trends (RI_{β_F}) using the following formula:

$$RI_{\beta_F} = \left(\frac{a\beta_F}{\beta_{NDVImax}} \right) \times 100$$

We displayed the distribution of GSL, $\Sigma_{OBS_{GS}}$, $a\beta_F$, $r\beta_F$, $\beta_{NDVImax}$, and RI_{β_F} along an elevation gradient from 1500 to 2800 m a.s.l. In addition, we used the floristic surveys database from the French National Alpine Botanical Conservatory (CBNA) comprising n = 21 934 vegetation plots, from which we selected those above 1500 m a.s.l., with a geolocation accuracy < 20 m and which was sampled after 1990, resulting in n = 11 114 plots distributed in the French Alps. We conducted a similarity-based cluster analysis on the whole floristic datasets. Distances among plots were estimated with the Euclidean binary distance based on presence/absence data. For the clustering, we used the PAM algorithm with K = 12 and interpreted corresponding habitats based on the 20 most frequent species, capturing habitats ranging from alpine snowbed communities to the forest ecotone. We extracted all metrics described above for the 12 clusters and displayed their respective distribution.

Results

NDVImax sampling biases cause false greening trends

We confirmed that estimates of NDVImax depend on OBS_{GS} following an asymptotic relationship with the magnitude of the underestimation for low number of observations being related to the phenological curve (Fig. 3a) as initially shown by Berner et al. (2020). For example, with one observation, NDVImax was underestimated by an average of 30% for late snowmelting sites and 11% for early snowmelting sites. We found similar results using quantile metrics instead of maximum NDVI with a clear asymptotic relationship between the underestimation of vegetation greenness and OBS_{GS} (Supporting information). We tested nine methods to compute quantiles with none resulting in a diminution of the sampling bias (Supporting information). In addition, we found that the randomization of observation dates led to slight overestimation of the sampling bias compared to using the actual observation DOY, but with no redhibitory consequences on the main analysis (Supporting information). We applied the 38-year time series of OBS_{GS} over pixels from early, intermediate, and late snowmelting sites and evaluated how NDVImax sampling bias affects greenness trends estimates (Fig. 3B–F). Estimates of NDVImax varied from year to year simply because of the variation in OBS_{GS} Fig. 3B–D). Because OBS_{GS} increased over time (Fig. 1, 3B–D), the systematic underestimation of NDVImax decreases over time, leading to positive NDVImax trends ($a\beta_F$) that vary in magnitude depending on the timing of snowmelt (Fig. 3E). At the beginning of the Landsat time series, early snowmelting sites averaged $OBS_{GS} = 3$ (Fig. 3B), whereas late snowmelting sites averaged $OBS_{GS} = 2$. Therefore, the early snowmelting

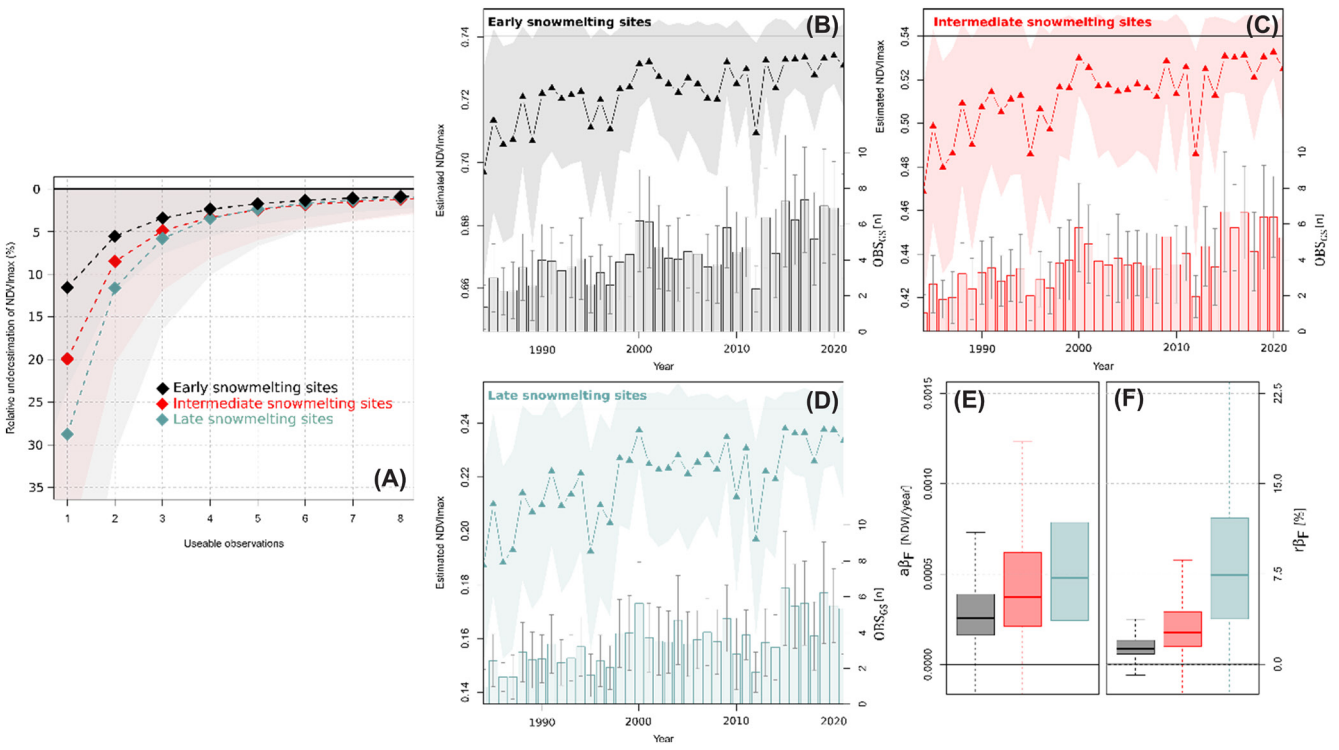

Figure 3. (A) Relative underestimation of NDVImax as a function of the number of usable observations during the growing season. Each dashed line depicts the median bias for a specific profile of snowmelting sites, while the shaded area depicts interquartile ranges. (B–D) Represent estimates of average annual maximum NDVI time series based on the number of usable Landsat observations during the growing season for early, intermediate, and late snowmelting sites, respectively. Histograms represent time series of OBS_{GS}. (E–F) Represent the resulting magnitude of absolute and relative false trends respectively for early, intermediate, and late snowmelting sites.

were less affected by the NDVImax sampling bias (Fig. 3A), resulting in less underestimation of NDVImax and thus lower false trends ($\beta_F = 0.00025$ NDVI year^{-1} versus $\beta_F = 0.00054$ NDVI year^{-1}). In term of relative false trends ($r\beta_F$), late snowmelting sites had an average increase in NDVImax of 7.5% due only to the variability of OBS_{GS} over time compared to only 2% for early snowmelting sites (Fig. 4F).

Observation density and phenology co-drive the magnitude of false NDVImax trends

We managed to explain 96% of variance in $a\beta_F$ using $\Sigma_{OBS_{GS}}$ and GSL as predictor variables in a random forest regression model with a root mean square error of 9.24×10^{-5} [8.29×10^{-5} to 9.81×10^{-5}]. We found $\Sigma_{OBS_{GS}}$ was slightly more important than GSL (%IncMSE of 1.5×10^{-7} and 1×10^{-7} for $\Sigma_{OBS_{GS}}$ and GSL, respectively) (Fig. 4A). Within the GSL and $\Sigma_{OBS_{GS}}$ range of values (100–170 and 50–300, respectively), $a\beta_F$ magnitude varied asymptotically from 0 to 0.0015 NDVI year^{-1} with higher magnitudes obtained with short growing season and limited observation density (Fig. 4B).

Higher false trends in late snowmelting ecosystems

GSL decreases almost linearly with elevation, ranging from almost 200 days at 1500 m to 110 days at 2800 m, while $\Sigma_{OBS_{GS}}$ shows a similar pattern but with an abrupt break point at approximately 2300 m and value ranging between 150 observations at 1500 m to 70 observations at 2800 m (Fig. 5A). Random forest model regression was used to estimate $a\beta_F$ for the entire European Alps between 1500 and 2800 m a.s.l. As a result, $a\beta_F$ increases steadily with elevation up to 2300 m ($a\beta_F < 0.0005$ NDVI year^{-1}) where it accelerates until 2600 m, reaching a value of almost 0.001 NDVI year^{-1} (Fig. 5B). Because NDVImax decreases with increasing elevation, $r\beta_F$ is limited until 2400 m ($r\beta_F < 5\%$) then increases linearly with elevation ($r\beta_F = 13\%$ at 2800 m, Fig. 5B). Observed trends in NDVImax at the scale of the European Alps show high magnitudes between 2200 and 2400 m ($\beta_{NDVImax} = 0.0029$ NDVI year^{-1}), and lower magnitudes at 1400 and 3000 m ($\beta_{NDVImax} = 0.0017$ and 0.0012 NDVI year^{-1}, respectively) (Fig. 5C). We found the relative importance of false trends increases linearly with elevation from 10 to 20% between 1500 and 2400 m, where it accelerates with a relative importance of 20–50% between 2400 and 2800 m (Fig. 5C). The median ranges of GSL for floristic clusters span from 127 [119–137] to 166 [151–182] for north-exposed alpine screes (cluster 2) and forest ecotone (cluster 12), respectively, and $\Sigma_{OBS_{GS}}$ ranges from ranges from 128 [103–163] to 225 [182–265]. Cluster 3, 4, 6 and 9 GSL and $\Sigma_{OBS_{GS}}$ ranged intermediately (Fig. 6A). Variability in GSL and $\Sigma_{OBS_{GS}}$ among plant communities resulted in variability in $a\beta_F$ with median values ranging from 0.0004 NDVI year^{-1} [0.0002–0.0007] for north-exposed alpine screes to 0.0002 NDVI year^{-1} [0.0001–0.0003] for forest ecotone (Fig. 6B). It led to RI_{β_F} up to 30% [12–50] for north-exposed alpine screes while only of 8% [5–12] for forest ecotone.

Discussion

Our study shows the increasing availability of Landsat observations over the historical record affects annual summaries of vegetation greenness in seasonally snow-covered environments, leading to false greening trends that confound efforts

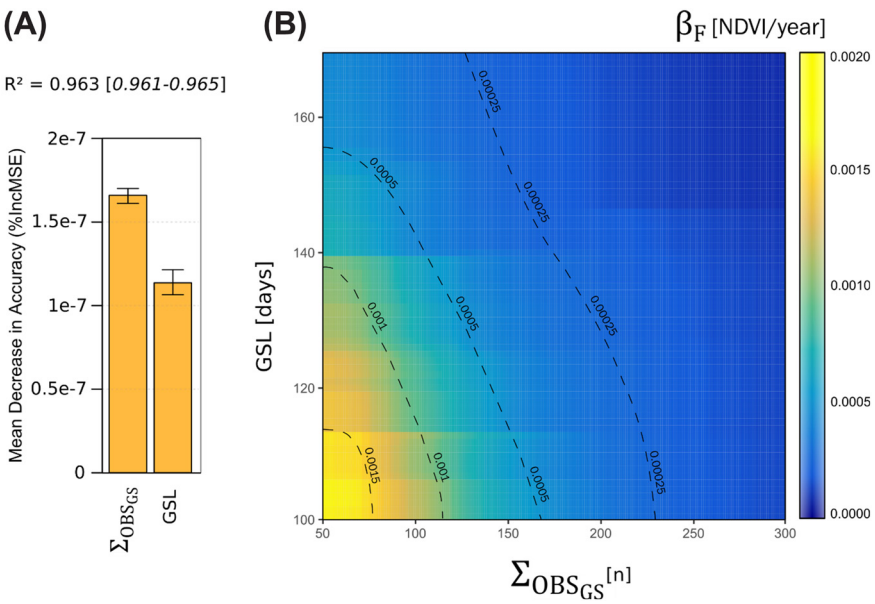

Figure 4. (A) Variable importance of $\Sigma_{OBS_{GS}}$, GSL, NDVImax, and Peakiness from a random forest regression model based on the measure of mean decrease in accuracy. Explained variance (measured as R^2) is given above with its interquartile range. (B) Bivariate partial dependence plot for $a\beta_F$ with the two most important predictive variables ($\Sigma_{OBS_{GS}}$ and GSL).

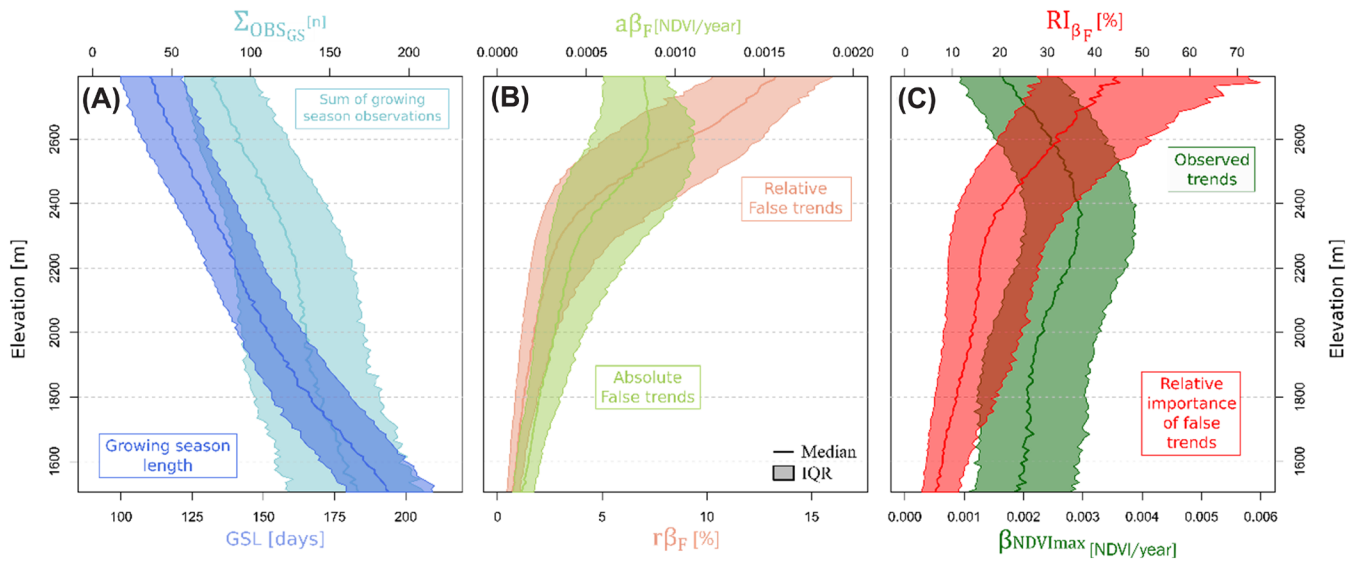

Figure 5. Distribution of (A) growing season length (GSL) and sum of growing season observations ($\Sigma_{OBS_{GS}}$). (B) Absolute ($a\beta_F$) and relative ($r\beta_F$) false trends and (C) observed trends ($\beta_{NDVImax}$) and relative importance of false trends ($RI_{\beta F}$), along elevation gradient ranging from 1500 to 2800 m a.s.l.

to understand multi-decadal vegetation responses to climate change, particularly in climate-sensitive, high-alpine environments. Specifically, we confirmed that annual estimates of maximum NDVI systematically increase with the number of available observations per growing season, as previously shown for the Arctic (Berner et al. 2020, 2023), while further showing that other annual metrics (e.g. median NDVI) are similarly affected. Focusing on the European Alps, we then demonstrated how the increasing availability of observations over the past four decades led to false greening trends associated with the sampling biases and, moreover, that the magnitude of these false greening trends was highest in areas with the lowest observation density and shortest growing season length. For instance, almost 50% of the observed greening trend in high-elevation alpine grasslands was due solely to this effect, though this effect was less pronounced in lower-elevation forest ecotone communities. Annual metrics of vegetation greenness are increasingly being derived from Landsat data (Bayle et al. 2022, Rumpf et al. 2022); however, our study underscores that caution is needed when deriving and analysing annual metrics of vegetation greenness using these satellites. To rigorously quantify multi-decadal changes in vegetation greenness, and likely other biophysical parameters, it is necessary to account for the effects of changes in observation availability throughout the Landsat record.

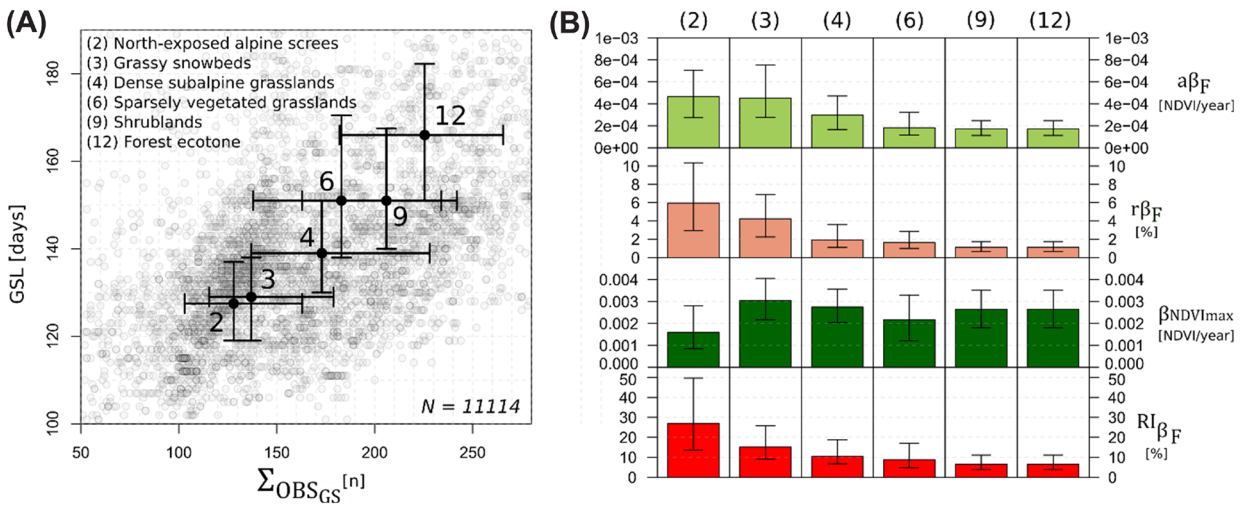

Figure 6. (A) Distribution of floristic plots (n = 11 114) along GSL and $\Sigma_{OBS_{GS}}$ gradients with median cluster position shows as black points. Ranges correspond to interquartile ranges. Only clusters used in (B) are shown in (A) to improve clarity. (B) Distribution of $a\beta_F$, $r\beta_F$, $\beta_{NDVImax}$, and $RI_{\beta F}$ for north-exposed alpine screes (2), grassy snowbeds (3), dense subalpine grasslands (4), sparsely vegetated grasslands (6), shrublands (9), and forest ecotone (12).

Implications for relating greening trends to ecological processes

Arithmetically derived estimates of annual maximum NDVI are impacted by sampling bias, leading to false greening trends in subsequent time series analyses. Consequently, by not considering the effect of sampling bias, the ecological interpretation of the greening observed by Landsat turns out to be partly erroneous. For example, when compared to the actual greening observed based on our computation and those of Rumpf et al. (2022) (Supporting information), the false trends might correspond to more than 50% of the observed greening in the alpine zone (> 2400 m a.s.l.) of the European Alps. This might explain why Rumpf et al. (2022) found a significantly higher proportion of surfaces were greening (77%) compared to previous studies (55%) that used MODIS satellites (Choler et al. 2021). Nevertheless, it is crucial to note that our demonstration in no way calls into question the overall greening of the European Alps, repeatedly demonstrated by several satellites and in many different contexts (Carlson et al. 2017, Bayle 2020, Choler et al. 2021, Rumpf et al. 2022, Bayle et al. 2023, Dentant et al. 2023), as the absolute values of the false trends we obtained are systematically lower than the trends observed without correction (Fig. 5, Supporting information).

Growing season length and Landsat observation availability are the two parameters influencing the magnitude of the false greening trends (Fig. 4), while exhibiting spatial variability (Fig. 5). In complex terrain, vegetation phenology is highly variable over short distances because of varying snow cover duration, thus the difficulty of capturing the true seasonal maximum NDVI can also vary over short distances (Dedieu et al. 2016, Choler 2018). In addition, the number of usable observations over the growing season varies along these same gradients. During the growing season in the European Alps, cloud cover affects an average of ~ 25% of Landsat observations, but up to 50% at the highest elevations (Hu et al. 2019). Furthermore, usable observations tend to decrease with increasing elevation because of poorly performing cloud masks that erroneously assume similar temperature from all clear-sky observations in one image, resulting in misclassification of cold surfaces as clouds (Qiu et al. 2017). High-elevation alpine ecosystems are particularly affected by false greening trends because of the late snowmelt dates and limited observations, while also being among the most threatened by climate warming (Engler et al. 2011, Gottfried et al. 2012, Steinbauer et al. 2018). One of the most striking examples is that of snowbed communities, which are particularly sensitive to climate and snow cover regime changes (Hiller et al. 2005, Schöb et al. 2008, Matteodo et al. 2016) and strongly affected by false greening trends (Fig. 6). Monitoring these endangered habitats is crucial to guide conservation policies, yet long-term surveys are generally lacking. Landsat time series are an ideal candidate for tracking the long-term response of these habitats. Yet, we showed that not accounting for NDVImax sampling bias and resulting false greening trends could have detrimental consequences for understanding changes that are occurring in these habitats (Fig. 6). Beyond snowbed communities, which represent an extreme case in terms of bias magnitude, the increase in bias magnitude with elevation might limit our ability to study the upward migration of warm-adapted species (i.e. thermophilisation) using the Landsat time series, as greening at higher elevation compared to lower elevation could be solely explained by the bias (Gottfried et al. 2012, Rosbakh et al. 2014, Dentant et al. 2023).

Our study did not consider the possibility of long-term increases in growing season length or reductions in snow cover, which could increase the number of usable observations and lead to better estimates of NDVImax at the end of the Landsat time. Over recent decades, climate change has led to longer growing seasons throughout the Northern Hemisphere (Jeong et al. 2011, Park et al. 2016, Piao et al. 2019). In cold regions, many studies have highlighted the reduction of snow cover duration during recent decades with various magnitudes depending on the region and elevation (Brown et al. 2010, Callaghan et al. 2012, Hernández-Henríquez et al. 2015, Mudryk et al. 2020). For example, the Eurasian Arctic region experienced larger declines in the duration of the snow-covered period (12.6 days), compared to the North American Arctic region (6.2 days) between 1982 and 2011 (Barichivich et al. 2013), though both changes could affect the magnitude of false greening trends (Fig. 5). For global mountains, shortening of the snow cover duration is observed across elevations albeit with various magnitudes (Immerzeel et al. 2009, Klein et al. 2016, Beaumet et al. 2021, Notarnicola 2022, Monteiro and Morin 2023). This additional temporal and spatial variability in changing snow cover duration and growing season length is expected to add complexity that was not accounted for in our analysis.

In this study, we evaluated false and observed greening trends based on linear changes over the entire Landsat period. However, recent studies show high temporal variability in NDVI trends, with phases of greening, stability, and even browning (Phoenix and Bjerke 2016). While overall greening has been observed during the last 40 years on a global scale, there is pronounced spatial variability and local reversals towards browning seem to be increasingly observed in part due to air temperature approaching or exceeding its optimum for vegetation and increasing moisture limitation (Keenan and Riley 2018, Huang et al. 2019, Winkler et al. 2021). In cold regions where Landsat is the most relevant tool to study these patterns (Ju and Masek 2016, Berner et al. 2020, Berner and Goetz 2022), local reversals from greening to browning have been documented (Phoenix and Bjerke 2016). These observations tend to push research towards further consideration of the temporal heterogeneity and non-linear trends in vegetation greenness dynamics (Wolkovich et al. 2014, Vickers et al. 2016, Bayle et al. 2022).

The Landsat history of increasing observation is itself non-linear and occurred mostly at two moments, when Landsat 7 ETM+ and Landsat 8 OLI came into operation in 1999 and 2013, respectively. Therefore, changes in the sampling bias likely occur non-linearly within the Landsat observation

period. Bayle et al. (2022) studied the temporal heterogeneity of Landsat-based greening trends while not accounting for the sampling bias in northeastern Canada, and found the occurrence of two distinct waves of greening, centred around 1996 and 2011. Both waves occurred at these Landsat transition periods, and while the first one was found to be highly correlated with rising summer temperatures, leaving little doubt to its ecological relevance, the second was not. Over their study site, $\Sigma_{OBS_{GS}}$ is approximately equal to 125 with GSL of 100 days, which suggests the presence of non-negligible NDVImax sampling bias (Fig. 4, 6). Given that the trend of the second greening wave ($\beta_{NDVImax} = 0.0075$ NDVI year^{-1}) was close to the average bias magnitude of 0.001 NDVI year^{-1} found under these conditions in the European Alps (Fig. 4), it is possible that the result did not reflect ecological change on the ground and instead was caused solely by increasing observation availability. This specific case is an example of how, if unaccounted for, this bias hampers our ability to interpret and understand ongoing ecological processes using remote sensing approaches.

False trends consideration for cold ecosystems worldwide

While our study focused on the European Alps and above-forest alpine vegetation, the combined effects of increased Landsat observation availability over time and short growing season length is found in cold ecosystems worldwide (Zhang et al. 2022). At a biogeographical scale, variation in Landsat observations comes from the combined effects of Landsat history (e.g. SCL failure) and topoclimatic patterns (see the Supporting information for Arctic and Asian mountains ranges example). For instance, the north American subarctic has particularly high observation density in the 1990s compared to other adjacent subarctic regions that have similar values as observed in the European Alps (Fig. 1, Supporting information). Nevertheless, the North American subarctic shows contrasting patterns with higher observation frequency in the inner Canadian Plains compared to Alaska or Nunavik. This spatial variability is attributable to several local factors. For example, Alaska suffered from the data relay problem and limited tasking before 1999 (Goward et al. 2006), while two ground receiving stations were in full operation in Canada (White and Wulder 2014), resulting in significant differences in observation availability (Ju and Masek 2016). At the same time, continentality affects cloud cover distribution, resulting in limited observations in, for example, Nunavik (Supporting information). Similar to alpine ecosystems, growing season length varies drastically along latitude and topography gradients in subarctic to high Arctic regions. Because the Landsat time series has increasing observation over time with large spatial variability in its magnitude, these underlying patterns could explain part of the spatial variability in Landsat-based vegetation greening trends. The AVHRR satellite time series also has inconsistent observation numbers over time (Dech et al. 2021). Hence, it is possible that differences between the Landsat and AVHRR satellites in spatial patterns of vegetation greening across North America (Ju and Masek 2016) could partially be due to satellite-specific changes in observations availability over time. In the mountains of Asia, there are very few observations at the beginning of the time series, whereas at the end of the series the number is equivalent to that of the other cold ecosystems presented (Supporting information). Thus, the trends in the increase in the number of observations are much more acute, suggesting a potentially greater bias. Furthermore, in certain climatic contexts, such as the Austrian Alps, higher cloud cover can coincide with peak vegetation, making it more difficult to capture NDVImax than in the southern Alps. Although our analysis focused on the European Alps, the mechanisms behind the emergence of false trends (increasing number of observations over time, low observation density, and short growing season length) can be found throughout the cold ecosystems of the Northern Hemisphere (Fig. 1, Supporting information). Overall, spatial variability in observation and phenology lead to spatial variation in the sampling bias magnitude and importance, which might hinder our understanding of spatial variability in greening trends (Myers-Smith et al. 2020).

Corrections or solutions proposed in the literature

The effects of sampling bias on phenological metrics like maximum NDVI can be addressed by either an avoidance or a correction strategy. While the sampling bias is expected to affect all terrestrial surfaces because of global patterns of increasing image availability over time (Fig. 1, Supporting information), we have shown that it only becomes a serious problem in certain cases (Fig. 5, Supporting information). For example, several studies have limited their analysis to years with sufficient observations (Frost et al. 2014, Carlson et al. 2017, Raynolds et al. 2018, Dentant et al. 2023), while others limited the study areas to overlapping tiles (Fraser et al. 2011). If skewed surfaces cannot be avoided, i.e. above 2400 m in the European Alps (Fig. 6), corrections have to be considered. Correcting for the bias means reconstructing or constructing missing information from information available elsewhere, a field in which the literature is flourishing. According to Shen et al. (2015), reconstruction approaches can be classified into three categories depending on the additional information used: 1) spatial-based methods, 2) spectral-based methods, and 3) temporal-based methods. In our case, as the missing information is often outside satellite acquisitions, the first two methods are generally ineffective. Temporal reconstruction can either be based on subsequent information, assuming regular chronological fluctuation (Chen et al. 2004, Beck et al. 2006, Viovy et al. 2007), or additional information, using data fusion methods (Gao et al. 2006, Zhu, X. et al. 2016, Zhu, Z. et al. 2016, Li et al. 2021, Qiu et al. 2021). In the first case, a Landsat-based temporal interpolation approach first fits a time series model to the original Landsat NDVI data and then predicts NDVI values on regular temporal intervals (Kovalskyy and Henebry 2012, Melaas et al. 2013, Zhu et al. 2015, Yan and Roy 2020,

Zhang et al. 2021). This approach was used by Berner et al. (2020) to correct for NDVImax estimation before computing trends in vegetation greenness across the Arctic. They developed a phenology-based approach by modelling the per pixel land surface phenology over a 17-year moving period to predict annual NDVImax and demonstrated the effectiveness of the correction. This approach has been effectively used with other spectral indices, e.g. EVI2, kNDVI (Berner and Goetz 2022), and is implemented in the 'LandsatTS' software package for R (Berner et al. 2023). In the second case, Landsat spatiotemporal fusion with another satellite of coarser spatial resolution but higher temporal resolution is a popular technique for reconstructing Landsat NDVI time series (Moreno-Martinez et al. 2020, Chen et al. 2021). In complex landscapes only MODIS could provide adequate spatial resolution, but data are not available before 2000. AVHRR products have too coarse a resolution and have been shown to be of limited use in correcting the bias, even in a forestry context (Wang et al. 2022). With the openings of the SPOT World Heritage archives in 2015, these non-systematic acquisition products might offer interesting possibilities to densify NDVI time series before applying a temporal filter (Barrou Dumont et al. 2023).

Conclusion

In this study, we quantified the effect of increasing Landsat observations availability on estimates of vegetation greenness trends during recent decades. We showed the increases in observation availability over time can lead to strong false greening trends when using maximum observed NDVI as a metric of annual vegetation greenness. The magnitude of these false trends are a function of observation density and growing season length, and while we focused on the European Alps, our analysis strongly suggests this methodological issue also affects other cold seasonally snow-covered ecosystems worldwide. Although we focused on vegetation greenness in seasonally snow-covered environments, this sampling bias can also likely create false trends in other biophysical parameters with seasonal variability such as the extent of the snow cover, flooded areas, and burnt areas, and hence warrants further investigation. We urge the scientific community to take this bias into account, or at the very least, to question their stationary conditions of seasonality and observation density prior to calculating and interpreting Landsat-based trends.

Acknowledgements – Editorial assistance, in the form of language editing and correction, was provided by Brad Z. Carlson.
Funding – This work received funding from the Agence Nationale de la Recherche (ANR) in the framework of the project TOP, Trajectories of agrO-Pastoral systems in mountains (ANR-20-CE32-0002). LECA is part of the Recherche Labex OSUG@2020 (IA-10-LABX-0056). LTB was supported by the National Aeronautics and Space Administration (NASA) Arctic Boreal Vulnerability Experiment (ABoVE) under grant no. 80NSSC22K1247 and the NASA Early Career Investigator Program in Earth Science under grant no. 80NSSC21K1364.

Author contributions

Arthur Bayle: Conceptualization (lead); Data curation (lead); Formal analysis (lead); Investigation (lead); Methodology (lead); Writing – original draft (lead); Writing – review and editing (lead). **Simon Gascoin**: Conceptualization (supporting); Data curation (supporting); Methodology (supporting); Writing – original draft (supporting); Writing – review and editing (supporting). **Logan T. Berner**: Methodology (supporting); Validation (supporting); Writing – review and editing (supporting). **Philippe Choler**: Conceptualization (supporting); Data curation (supporting); Funding acquisition (supporting); Methodology (supporting); Resources (supporting); Supervision (supporting); Writing – review and editing (supporting).

Transparent peer review

The peer review history for this article is available at https://www.webofscience.com/api/gateway/wos/peer-review/10.1111/ecog.07394.

Data availability statement

Data are available from the Dryad Digital Repository: https://doi.org/10.5061/dryad.1rn8pk13f (Bayle et al. 2024).

Supporting information

The Supporting information associated with this article is available with the online version.

References

Anderson, K., Fawcett, D., Cugulliere, A., Benford, S., Jones, D. and Leng, R. 2020. Vegetation expansion in the subnival Hindu Kush Himalaya. – Global Change Biol. 26: 1608–1625.
Arvidson, T., Goward, S., Gasch, J. and Williams, D. 2006. Landsat-7 long-term acquisition plan: development and validation. – Photogramm. Eng. Remote Sens. 72: 1137–1146.
Assmann, J. J., Myers-Smith, I. H., Kerby, J. T., Cunliffe, A. M. and Daskalova, G. N. 2020. Drone data reveal heterogeneity in tundra greenness and phenology not captured by satellites. – Environ. Res. Lett. 15: 125002.
Barichivich, J., Briffa, K. R., Myneni, R. B., Osborn, T. J., Melvin, T. M., Ciais, P., Piao, S. and Tucker, C. 2013. Large-scale variations in the vegetation growing season and annual cycle of atmospheric CO_2 at high northern latitudes from 1950 to 2011. – Global Change Biol. 19: 3167–3183.
Barrou Dumont, Z., Gascoin, S. and Inglada, J. 2023. Contribution de SPOT World Heritage aux séries temporelles d'observation satellitaires des montagnes françaises. – Rev. Fr. Photogramm. Télédétection 225: 1–8.
Bayle, A. 2020. A recent history of deglaciation and vegetation establishment in a contrasted geomorphological context, Glacier Blanc, French Alps. – J. Maps 16: 766–775.
Bayle, A., Roy, A., Dedieu, J.-P., Boudreau, S., Choler, P. and Lévesque, E. 2022. Two distinct waves of greening in northeastern Canada: summer warming does not tell the whole story. – Environ. Res. Lett. 17: 064051.

Bayle, A., Carlson, B. Z., Zimmer, A., Vallée, S., Rabatel, A., Cremonese, E., Filippa, G., Dentant, C., Randin, C., Mainetti, A., Roussel, E., Gascoin, S., Corenblit, D. and Choler, P. 2023. Local environmental context drives heterogeneity of early succession dynamics in alpine glacier forefields. – Biogeosciences 20: 1649–1669.

Bayle, A., Gascoin, S., Berner, L. T. and Choler, P. 2024. Data from: Landsat-based greening trends in alpine ecosystems are inflated by multidecadal increases in summer observations. – Dryad Digital Repository, https://doi.org/10.5061/dryad.1rn8pk13f.

Beaumet, J., Ménégoz, M., Morin, S., Gallée, H., Fettweis, X., Six, D., Vincent, C., Wilhelm, B. and Anquetin, S. 2021. Twentieth century temperature and snow cover changes in the French Alps. – Reg. Environ. Change 21: 114.

Beck, P. S. A., Atzberger, C., Høgda, K. A., Johansen, B. and Skidmore, A. K. 2006. Improved monitoring of vegetation dynamics at very high latitudes: a new method using MODIS NDVI. – Remote Sens. Environ. 100: 321–334.

Berner, L. T. and Goetz, S. J. 2022. Satellite observations document trends consistent with a boreal forest biome shift. – Global Change Biol. 28: 3275–3292.

Berner, L. T., Massey, R., Jantz, P., Forbes, B. C., Macias-Fauria, M., Myers-Smith, I., Kumpula, T., Gauthier, G., Andreu-Hayles, L., Gaglioti, B. V., Burns, P., Zetterberg, P., D'Arrigo, R. and Goetz, S. J. 2020. Summer warming explains widespread but not uniform greening in the Arctic tundra biome. – Nat. Commun. 11: 4621.

Berner, L. T., Assmann, J. J., Normand, S. and Goetz, S. J. 2023. 'LandsatTS': an R package to facilitate retrieval, cleaning, cross-calibration, and phenological modeling of Landsat time series data. – Ecography 2023: e06768.

Breiman, L. 2001. Random forests. – Machine Learning 45: 5–32. https://doi.org/10.1023/A:1010933404324.

Brown, R., Derksen, C. and Wang, L. 2010. A multi-data set analysis of variability and change in Arctic spring snow cover extent, 1967–2008. – J. Geophys. Res. 115: D16

Callaghan, T. V. et al. 2012. The changing face of arctic snow cover: a synthesis of observed and projected changes. – Ambio 40: 17–31.

Carlson, B. Z., Corona, M. C., Dentant, C., Bonet, R., Thuiller, W. and Choler, P. 2017. Observed long-term greening of alpine vegetation – a case study in the French Alps. – Environ. Res. Lett. 12: 114006.

Chen, J., Jönsson, P., Tamura, M., Gu, Z., Matsushita, B. and Eklundh, L. 2004. A simple method for reconstructing a high-quality NDVI time-series data set based on the Savitzky–Golay filter. – Remote Sens. Environ. 91: 332–344.

Chen, Y., Cao, R., Chen, J., Liu, L. and Matsushita, B. 2021. A practical approach to reconstruct high-quality Landsat NDVI time-series data by gap filling and the Savitzky–Golay filter. – ISPRS J. Photogramm. 180: 174–190.

Choler, P. 2018. Winter soil temperature dependence of alpine plant distribution: implications for anticipating vegetation changes under a warming climate. – Perspect. Plant Ecol. Evol. Syst. 30: 6–15.

Choler, P., Bayle, A., Carlson, B. Z., Randin, C., Filippa, G. and Cremonese, E. 2021. The tempo of greening in the European Alps: spatial variations on a common theme. – Global Change Biol. 27: 5614–5628.

Dech, S. et al. 2021. Potential and challenges of harmonizing 40 years of AVHRR data: the TIMELINE experience. – Remote Sens. 13: 3618.

Dedieu, J.-P., Carlson, B., Bigot, S., Sirguey, P., Vionnet, V. and Choler, P. 2016. On the importance of high-resolution time series of optical imagery for quantifying the effects of snow cover duration on alpine plant habitat. – Remote Sens. 8: 481.

Dentant, C., Carlson, B. Z., Bartalucci, N., Bayle, A. and Lavergne, S. 2023. Anthropocene trajectories of high alpine vegetation on Mont-Blanc nunataks. – Bot. Lett. 171: 65–79.

Engler, R. et al. 2011. 21st century climate change threatens mountain flora unequally across Europe. – Global Change Biol. 17: 2330–2341.

Fraser, R. H., Olthof, I., Carrière, M., Deschamps, A. and Pouliot, D. 2011. Detecting long-term changes to vegetation in northern Canada using the Landsat satellite image archive. – Environ. Res. Lett. 6: 045502.

Frost, G. V., Epstein, H. E. and Walker, D. A. 2014. Regional and landscape-scale variability of Landsat-observed vegetation dynamics in northwest Siberian tundra. – Environ. Res. Lett. 9: 025004.

Gao, F., Masek, J., Schwaller, M. and Hall, F. 2006. On the blending of the Landsat and MODIS surface reflectance: predicting daily Landsat surface reflectance. – IEEE Trans. Geosci. Remote Sens. 44: 2207–2218.

Goetz, S. J., Bunn, A. G., Fiske, G. J. and Houghton, R. A. 2005. Satellite-observed photosynthetic trends across boreal North America associated with climate and fire disturbance. – Proc. Natl Acad. Sci. USA 102: 13521–13525.

Gottfried, M. et al. 2012. Continent-wide response of mountain vegetation to climate change. – Nat. Clim. Change 2: 111–115.

Goward, S., Arvidson, T., Williams, D., Faundeen, J., Irons, J. and Franks, S. 2006. Historical record of Landsat global coverage: mission operations, NSLRSDA, and international cooperator stations. – Photogramm. Eng. Remote Sens. 72: 1155–1169.

Hernández-Henríquez, M. A., Déry, S. J. and Derksen, C. 2015. Polar amplification and elevation-dependence in trends of Northern Hemisphere snow cover extent, 1971–2014. – Environ. Res. Lett. 10: 044010.

Hiller, B., Nuebel, A., Broll, G. and Holtmeier, F.-K. 2005. Snowbeds on silicate rocks in the upper Engadine (central Alps, Switzerland) – pedogenesis and interactions among soil, vegetation, and snow cover. – Arct. Antarct. Alp. Res. 37: 465–476.

Holben, B. N. 1986. Characteristics of maximum-value composite images from temporal AVHRR data. – Int. J. Remote Sens. 7: 1417–1434.

Hu, Z., Dietz, A. and Kuenzer, C. 2019. The potential of retrieving snow line dynamics from Landsat during the end of the ablation seasons between 1982 and 2017 in European mountains. – Int. J. Appl. Earth Obs. Geoinf. 78: 138–148.

Huang, M. et al. 2019. Air temperature optima of vegetation productivity across global biomes. – Nat. Ecol. Evol. 3: 772–779.

Hyndman, R. J. and Fan, Y. 1996. Sample quantiles in statistical packages. – Am. Stat. 50: 361–365. https://doi.org/10.2307/2684934

Immerzeel, W. W., Droogers, P., de Jong, S. M. and Bierkens, M. F. P. 2009. Large-scale monitoring of snow cover and runoff simulation in Himalayan river basins using remote sensing. – Remote Sens. Environ. 113: 40–49.

Ives, A. R., Zhu, L., Wang, F., Zhu, J., Morrow, C. J. and Radeloff, V. C. 2021.Statistical inference for trends in spatiotemporal data. – Remote Sensing Enviro. 2021: 112678. https://doi.org/10.1016/j.rse.2021.112678

Jeong, S.-J., Ho, C.-H., Gim, H.-J. and Brown, M. E. 2011. Phenology shifts at start vs. end of growing season in temperate vegetation over the Northern Hemisphere for the period 1982–2008. – Global Change Biol. 17: 2385–2399.

Ju, J. and Roy, D. P. 2008. The availability of cloud-free Landsat ETM+ data over the conterminous United States and globally. – Remote Sens. Environ. 112: 1196–1211.
Ju, J. and Masek, J. G. 2016. The vegetation greenness trend in Canada and US Alaska from 1984–2012 Landsat data. – Remote Sens. Environ. 176: 1–16.
Karlsen, S. R., Anderson, H. B., van der Wal, R. and Hansen, B. B. 2018. A new NDVI measure that overcomes data sparsity in cloud-covered regions predicts annual variation in ground-based estimates of high arctic plant productivity. – Environ. Res. Lett. 13: 025011.
Keenan, T. F. and Riley, W. J. 2018. Greening of the land surface in the world's cold regions consistent with recent warming. – Nat. Clim. Change 8: 825–828.
Klein, G., Vitasse, Y., Rixen, C., Marty, C. and Rebetez, M. 2016. Shorter snow cover duration since 1970 in the Swiss Alps due to earlier snowmelt more than to later snow onset. – Clim. Change 139: 637–649.
Kovalskyy, V. and Henebry, G. M. 2012. A new concept for simulation of vegetated land surface dynamics – Part 1: the event driven phenology model. – Biogeosciences 9: 141–159.
Kovalskyy, V. and Roy, D. P. 2013. The global availability of Landsat 5 TM and Landsat 7 ETM+ land surface observations and implications for global 30m Landsat data product generation. – Remote Sens. Environ. 130: 280–293.
Krishnaswamy, J., John, R. and Joseph, S. 2014. Consistent response of vegetation dynamics to recent climate change in tropical mountain regions. – Global Change Biol. 20: 203–215.
Lee, D. S., Storey, J. C., Choate, M. J. and Hayes, R. W. 2004. Four years of Landsat-7 on-orbit geometric calibration and performance. – IEEE Trans. Geosci. Remote Sens. 42: 2786–2795.
Li, X., Ling, F., Foody, G. M., Boyd, D. S., Jiang, L., Zhang, Y., Zhou, P., Wang, Y., Chen, R. and Du, Y. 2021. Monitoring high spatiotemporal water dynamics by fusing MODIS, Landsat, water occurrence data and DEM. – Remote Sens. Environ. 265: 112680.
Loveland, T. R., Anderson, M. C., Huntington, J. L., Irons, J. R., Johnson, D. M., Rocchio, L. E. P., Woodcock, C. E. and Wulder, M. A. 2022. Seeing our planet anew: fifty years of landsat. – Photogramm. Eng. Remote Sens. 88: 429–436.
Maechler, M., Rousseeuw, P., Struyf, A., Hubert, M. and Hornik, K. 2022. cluster: cluster analysis basics and extensions. – R package ver. 2.1.4, https://CRAN.R-project.org/package=clu.
Mallat, S. and Hwang, W. L. 1992. Singularity detection and processing with wavelets. – IEEE Trans. Inf. Theor. 38: 617–643.
Markham, B. L. and Helder, D. L. 2012. Forty-year calibrated record of earth-reflected radiance from Landsat: a review. – Remote Sens. Environ. 122: 30–40.
Masek, J. G., Wulder, M. A., Markham, B., McCorkel, J., Crawford, C. J., Storey, J. and Jenstrom, D. T. 2020. Landsat 9: empowering open science and applications through continuity. – Remote Sens. Environ. 248: 111968.
Matteodo, M., Ammann, K., Verrecchia, E. P. and Vittoz, P. 2016. Snowbeds are more affected than other subalpine-alpine plant communities by climate change in the Swiss Alps. – Ecol. Evol. 6: 6969–6982.
Mebane, W. R. and Sekhon, J. S. 2011. Genetic optimization using derivatives: the rgenoud package for R. – J. Stat. Softw. 42. 11 1–26
Melaas, E. K., Friedl, M. A. and Zhu, Z. 2013. Detecting interannual variation in deciduous broadleaf forest phenology using Landsat TM/ETM+ data. – Remote Sens. Environ. 132: 176–185.
Monteiro, D. and Morin, S. 2023. Multi-decadal analysis of past winter temperature, precipitation and snow cover data in the European Alps from reanalyses, climate models and observational datasets. – Cryosphere 17: 3617–3660.
Moreno-Martínez, Á., Izquierdo-Verdiguier, E., Maneta, M. P., Camps-Valls, G., Robinson, N., Muñoz-Marí, J., Sedano, F., Clinton, N. and Running, S. W. 2020. Multispectral high resolution sensor fusion for smoothing and gap-filling in the cloud. – Remote Sens. Environ. 247: 111901.
Mudryk, L., Santolaria-Otín, M., Krinner, G., Ménégoz, M., Derksen, C., Brutel-Vuilmet, C., Brady, M. and Essery, R. 2020. Historical Northern Hemisphere snow cover trends and projected changes in the CMIP6 multi-model ensemble. – Cryosphere 14: 2495–2514.
Myers-Smith, I. H. et al. 2020. Complexity revealed in the greening of the Arctic. – Nat. Clim. Change 10: 106–117.
Myneni, R. B., Keeling, C. D., Tucker, C. J., Asrar, G. and Nemani, R. R. 1997. Increased plant growth in the northern high latitudes from 1981 to 1991. – Nature 386: 698–702.
Notarnicola, C. 2022. Overall negative trends for snow cover extent and duration in global mountain regions over 1982–2020. – Sci. Rep. 12: 13731.
Park, T., Ganguly, S., Tømmervik, H., Euskirchen, E. S., Høgda, K.-A., Karlsen, S. R., Brovkin, V., Nemani, R. R. and Myneni, R. B. 2016. Changes in growing season duration and productivity of northern vegetation inferred from long-term remote sensing data. – Environ. Res. Lett. 11: 084001.
Phoenix, G. K. and Bjerke, J. W. 2016. Arctic browning: extreme events and trends reversing arctic greening. – Global Change Biol. 22: 2960–2962.
Piao, S., Liu, Q., Chen, A., Janssens, I. A., Fu, Y., Dai, J., Liu, L., Lian, X., Shen, M. and Zhu, X. 2019. Plant phenology and global climate change: current progresses and challenges. – Global Change Biol. 25: 1922–1940.
Qiu, S., He, B., Zhu, Z., Liao, Z. and Quan, X. 2017. Improving Fmask cloud and cloud shadow detection in mountainous area for Landsats 4–8 images. – Remote Sens. Environ. 199: 107–119.
Qiu, S., Zhu, Z., Olofsson, P., Woodcock, C. E. and Jin, S. 2023. Evaluation of Landsat image compositing algorithms. – Remote Sens. Environ. 285: 113375.
Qiu, Y., Zhou, J., Chen, J. and Chen, X. 2021. Spatiotemporal fusion method to simultaneously generate full-length normalized difference vegetation index time series (SSFIT). – Int. J. Appl. Earth Obs. Geoinf. 100: 102333.
Randin, C. F. et al. 2020. Monitoring biodiversity in the Anthropocene using remote sensing in species distribution models. – Remote Sens. Environ. 239: 111626.
Raynolds, M. K., Walker, D. A., Verbyla, D. and Munger, C. A. 2018. Patterns of change within a tundra landscape: 22-year Landsat NDVI trends in an area of the northern foothills of the Brooks Range, Alaska. – Arct. Antarct. Alp. Res. 45: 249–260.
Rosbakh, S., Bernhardt-Römermann, M. and Poschlod, P. 2014. Elevation matters: contrasting effects of climate change on the vegetation development at different elevations in the Bavarian Alps. – Alp. Bot. 124: 143–154.
Rouse, J. W., Haas, R. H., Schell, J. A. and Deering, D. W. 1974. Monitoring vegetation systems in the Great Plains with ERTS. – NASA Spec Publ 351, pp. 309–317.
Roy, D. P., Kovalskyy, V., Zhang, H. K., Vermote, E. F., Yan, L., Kumar, S. S. and Egorov, A. 2016a. Characterization of Landsat-7

to Landsat-8 reflective wavelength and normalized difference vegetation index continuity. – Remote Sens. Environ. 185: 57–70.
Roy, D. P., Zhang, H. K., Ju, J., Gomez-Dans, J. L., Lewis, P. E., Schaaf, C. B., Sun, Q., Li, J., Huang, H. and Kovalskyy, V. 2016b. A general method to normalize Landsat reflectance data to nadir BRDF adjusted reflectance. – Remote Sens. Environ. 176: 255–271.
Rumpf, S. B., Gravey, M., Brönnimann, O., Luoto, M., Cianfrani, C., Mariethoz, G. and Guisan, A. 2022. From white to green: snow cover loss and increased vegetation productivity in the European Alps. – Science 376: 1119–1122.
Savitzky, A. and Golay, M. J. E. 1964. Smoothing and differentiation of data by simplified least squares procedures. – Anal. Chem. 36: 1627–1639. DOI: 10.1021/ac60214a047
Schöb, C., Kammer, P. M., Choler, P. and Veit, H. 2008. Small-scale plant species distribution in snowbeds and its sensitivity to climate change. – Plant Ecol. 200: 91–104.
Shen, H., Li, X., Cheng, Q., Zeng, C., Yang, G., Li, H. and Zhang, L. 2015. Missing information reconstruction of remote sensing data: a technical review. – IEEE Geosci. Remote Sens. Mag. 3: 61–85.
Shukla, P. R. et al. 2019. Climate change and land: an IPCC special report on climate change, desertification, land degradation, sustainable land management, food security, and greenhouse gas fluxes in terrestrial ecosystems. – IPCC.
Steinbauer, M. J. et al. 2018. Accelerated increase in plant species richness on mountain summits is linked to warming. – Nature 556: 231–234.
Tucker, C. J. 1979. Red and photographic infrared linear combinations for monitoring vegetation. – Remote Sens. Environ. 8: 127–150.
Tucker, C. J. and Sellers, P. J. 1986. Satellite remote sensing of primary production. – Int. J. Remote Sens. 7: 1395–1416.
Vickers, H., Høgda, K. A., Solbø, S., Karlsen, S. R., Tømmervik, H., Aanes, R. and Hansen, B. B. 2016. Changes in greening in the high Arctic: insights from a 30 year AVHRR max NDVI dataset for Svalbard. – Environ. Res. Lett. 11: 105004.
Viovy, N., Arino, O. and Belward, A. S. 1992. The best index slope extraction (BISE): a method for reducing noise in NDVI time-series. – Int. J. Remote Sens. 13: 1585–1590.
Wang, C., Wang, A., Guo, D., Li, H. and Zang, S. 2022. Off-peak NDVI correction to reconstruct Landsat time series for post-fire recovery in high-latitude forests. – Int. J. Appl. Earth Obs. Geoinf. 107: 102704.
White, J. C. and Wulder, M. A. 2014. The Landsat observation record of Canada: 1972–2012. – Can. J. Remote Sens. 39: 455–467.
Winkler, A. J., Myneni, R. B., Hannart, A., Sitch, S., Haverd, V., Lombardozzi, D., Arora, V. K., Pongratz, J., Nabel, J. E. M. S., Goll, D. S., Kato, E., Tian, H., Arneth, A., Friedlingstein, P., Jain, A. K., Zaehle, S. and Brovkin, V. 2021. Slowdown of the greening trend in natural vegetation with further rise in atmospheric CO_2. – Biogeosciences 18: 4985–5010.
Wolkovich, E. M., Cook, B. I., McLauchlan, K. K. and Davies, T. J. 2014. Temporal ecology in the Anthropocene. – Ecol. Lett. 17: 1365–1379.
Wulder, M. A. et al. 2019. Current status of Landsat program, science, and applications. – Remote Sens. Environ. 225: 127–147.
Wulder, M. A. et al. 2022. Fifty years of Landsat science and impacts. – Remote Sens. Environ. 280: 113195.
Wulder, M. A., White, J. C., Loveland, T. R., Woodcock, C. E., Belward, A. S., Cohen, W. B., Fosnight, E. A., Shaw, J., Masek, J. G. and Roy, D. P. 2016. The global Landsat archive: status, consolidation, and direction. – Remote Sens. Environ. 185: 271–283.
Yan, L. and Roy, D. P. 2020. Spatially and temporally complete Landsat reflectance time series modelling: the fill-and-fit approach. – Remote Sens. Environ. 241: 111718.
Zhang, J., Shang, R., Rittenhouse, C., Witharana, C. and Zhu, Z. 2021. Evaluating the impacts of models, data density and irregularity on reconstructing and forecasting dense Landsat time series. – Sci. Remote Sens. 4: 100023.
Zhang, Y., Woodcock, C. E., Arévalo, P., Olofsson, P., Tang, X., Stanimirova, R., Bullock, E., Tarrio, K. R., Zhu, Z. and Friedl, M. A. 2022. A global analysis of the spatial and temporal variability of usable landsat observations at the pixel scale. – Front. Remote Sens. 3: 894618.
Zhu, X., Helmer, E. H., Gao, F., Liu, D., Chen, J. and Lefsky, M. A. 2016. A flexible spatiotemporal method for fusing satellite images with different resolutions. – Remote Sens. Environ. 172: 165–177.
Zhu, Z. and Woodcock, C. E. 2012. Object-based cloud and cloud shadow detection in Landsat imagery. – Remote Sens. Environ. 118: 83–94.
Zhu, Z., Woodcock, C. E., Holden, C. and Yang, Z. 2015. Generating synthetic Landsat images based on all available Landsat data: predicting Landsat surface reflectance at any given time. – Remote Sens. Environ. 162: 67–83.
Zhu, Z. et al. 2016. Greening of the Earth and its drivers. – Nat. Clim. Change 6: 791–795.